Soft Matter

Accepted Manuscript

ROYAL SOCIETY OF CHEMISTRY

www.rsc.org/softmatter

Journal Name

ARTICLE

Porous films by the self-assembly of inorganic rod-*b*-coil block copolymers. Mechanistic insights into the vesicle-to-pore morphological evolution.

Received 00th January 20xx,
Accepted 00th January 20xx

DOI: 10.1039/x0xx00000x

www.rsc.org/

Silvia Suárez-Suárez, Gabino A. Carriedo and Alejandro Presa Soto*

The self-assembly in thin films of the polyphosphazene block copolymers $[N=P(O_2C_{12}H_8)]_n$-*b*-$[N=PMePh]_m$ ($O_2C_{12}H_8$ = 2,2'-dioxy-1,1'-biphenyl; **2a**: *n* = 50, *m* = 35; **2b**: *n* = 20, *m* = 70, and **2c**: *n* = 245, *m* = 60), having different volume fractions of the rigid $[N=P(O_2C_{12}H_8)]_n$ block, has been studied. BCP **2a** spontaneously self-assembled into well-defined round-shaped macroporous films, observing also, as a minor morphology, spherical vesicles in regions where the film was no formed. A detailed study by SEM, TEM and AFM of the structure of the vesicles, the morphology of the pores (inverted mushroom-shaped), and the behaviour of the copolymers with shorter (**2b**) and longer (**2c**) $[N=P(O_2C_{12}H_8)]_n$ rigid blocks, provided sufficient experimental evidences to propose a vesicle-to-pore morphological evolution as the most likely mechanism to explain the pore formation during the self-assembly of **2a**. Moreover, by changing the volume fraction of the rigid block and the speed of solvent evaporation, it was possible to vary the pore morphology (and their diameter) from isolated regular groups to 3D interconnected pore networks.

Introduction.

Natural structures are a source of inspiration for scientist involved in different fields ranging from chemistry to material science. The variety of morphologies and hierarchical organizations originate intriguing properties that researchers try to mimic by using appropriate synthetic building blocks.[1] In this regard, the synthesis of nanostructured porous materials has attracted wide interest due to their applications in chemical sensors,[2] photonics,[3] membranes,[4] catalysis,[5] gas storage,[6] and biomedical science.[7] Among these materials, porous polymers show many advantages because they are easily processable, and can be conveniently functionalized into the porous framework or at the pore surface.[8,6b] The self-assembly of block copolymers (BCPs) is an invaluable tool for designing nanostructured materials,[9] including well-defined porous architectures.[10] BCPs can be used: (1) as pore templates that have to be removed (i.e. they are sacrificial components) after creating the porous textures (e.g., by thermal degradation[11] or solvent extraction[12]); or (2) as the source of the porous framework. In the latter approach the BCPs, or at least one of the blocks, remain in the final structure of the material.[13] Recently, a very convenient approach to porous materials has been developed based on the creation of well-defined hollow nanostructures in solution (vesicles) that evolve to porous films after their close-packed self-ordering during the solvent evaporation.[14] This hierarchical self-assembly represents a non-template approach to porous materials involving non-sacrificial components. For instance, Jenekhe and co-workers reported the formation of porous films by self-ordering of vesicles from rod-coil BCPs induced by the solvent evaporation.[15] Later, Fahmi *et al.* showed the formation of ordered porous films when solutions of metal loaded vesicles were spin-coated onto a solid substrate. Based on the dependence of the pore diameter with the size distribution of vesicles in solution, they proposed a two-step mechanism comprising first, the packing of vesicles that lead to the film formation, and second, the collapse of the vesicle membrane originating the pore.[16] Very recently, Novak and collaborators proposed a similar mechanism to explain the spontaneous formation of porous films when solutions of chiral rod-coil block copolymers were casted onto solid substrates.[17] Although they convincingly demonstrated the existence of vesicles in solution, the experimental evidences supporting the collapsing of the vesicles and the structure of the pores, were limited to the observation of protruding spherical hills by AFM that evolve to pores after a thermal annealing treatment. Therefore, a more in depth study is required to fully characterize the vesicle-to-pore morphological evolution. Our group has recently reported the spontaneous formation of porous films by the self-assembly of chiral rod-coil block copolyphosphazene (see BCP **1** in Figure 1).[18] While studying the influence of the chirality and the

S. Suárez-Suárez, Prof. G. A. Carriedo, Dr. A. Presa Soto
Química Orgánica e Inorgánica (IUQOEM)
Universidad de Oviedo
Julián Clavería s/n, 33006, Oviedo (Spain)
E-mail: presaalejandro@uniovi.es
† Footnotes relating to the title and/or authors should appear here.
Electronic Supplementary Information (ESI) available: [details of any supplementary information available should be included here]. See DOI: 10.1039/x0xx00000x

rigidity in the pore formation by using an analogous block copolyphosphazene having the rigid and non-chiral [N=P($O_2C_{12}H_8$)] block ($O_2C_{12}H_8$ = 2,2'-dioxy-1,1'-biphenyl, see BCP **2a** in Figure 1), we found experimental evidences (DLS, SEM, TEM and AFM) to characterize various intermediate morphologies during the vesicle-to-pore transformation, allowing the proposal of a morphological evolution pathway which was further supported by the self-assembly of BCPs **2b** and **2c** having respectively significantly different volume fractions of the rigid [N=P($O_2C_{12}H_8$)] block than that of **2a** (see Figure 1 and Table 1). Herein, we characterise the pore structure of **2a** and study their stability under the conditions required to ensure the chain mobility (thermal and solvent annealing), showing that the pores are kinetically trapped nanostructures.

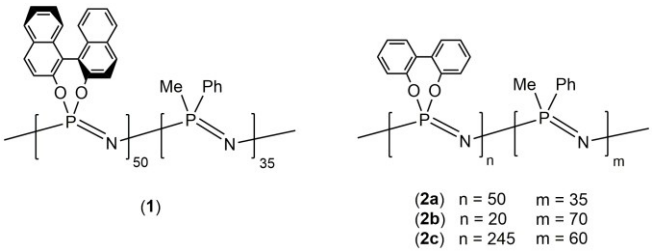

Figure 1. Chemical structures of polyphosphazene block copolymers **1** and **2a-c**.

Results and Discussion

The block copolymers **2a-c** were synthesized following a modified procedure[19] from that previously described by Allcock and collaborators.[20] Thus, using mono end-capped initiators, the block copolymers **2a-c** were isolated as white solids in good yields and with narrow molecular weight distributions (see Table 1 and SEC traces in Figure S1). The bulky and cyclic 2,2'-dioxy-1,1'-biphenyl phosphazene units, [N=P($O_2C_{12}H_8$)], provided the rigid (non-flexible) blocks. These blocks have a T_g of *ca*. 130 °C, with an activation energy at T_g of ΔH_{Tg} = 500 KJ mol^{-1}, which is in the range of high activation barriers characteristic of very rigid blocks.[21] Those blocks were combined with the much more flexible [N=PMePh]$_m$ segments (T_g *ca.* 37 °C). Being therefore the rigidity of the [N=P($O_2C_{12}H_8$)] blocks the main factor controlling the self-assembly of these materials, three block ratios were chosen ([N=P($O_2C_{12}H_8$)]$_n$-*b*-[N=PMePh]$_m$; **2a**: *n* = 50, *m* = 35; **2b**: *n* = 20, *m* = 70; **2c**: *n* = 245, *m* = 60), leading to significantly different materials having different volume fractions of rigid block (see Table 1).

Table 1. Characterization details of block copolymers **2a-c**.

BCP	M_n (g / mol)[a]	PDI[b]	Yield (%)	φ[N=P($O_2C_{12}H_8$)][c]
2a	2.4·10^4	1.3	56	0.66
2b	2.6·10^4	1.3	40	0.28
2c	6.3·10^4	1.2	60	0.85

[a]Number average molecular weight determined by GPC. [b] Polydispersity index determined by GPC. [c] Volume fraction of the rigid block (ρ [N=P($O_2C_{12}H_8$)] = 1.48 g / mL and ρ [N=PMePh] = 1.21 g / mL).

Dynamic Light Scattering (DLS) studies of the THF solutions of BCPs 2a-c. The self-assembly of BCPs **2a-c** were first studied using the same experimental conditions (solvent and concentration) previously optimised for the pore forming chiral block copolymer **1** (Figure 1).[18] Thus, solutions in THF (good solvent for both blocks)[22]of BCPs **2a-c** (10 mg mL^{-1}) were prepared. Dynamic light scattering (DLS) analysis showed two peaks: one at very low values of apparent hydrodynamic diameters [$D_{h,app}$ of 5 nm (**2a**, PDI = 0.15), 7 nm (**2b**, PDI = 0.13), and 9 nm (**2c**, PDI = 0.22)] which corresponded to non-aggregated (solvated) BCP chains; and other at higher values of $D_{h,app}$ [341 nm (**2a**, PDI = 0.17), 59 nm (**2b**, PDI = 0.14), and 1151 nm (**2c**, PDI = 0.32)], evidencing the presence of aggregates in solution (Figure 2). The aggregation was very significant in BCPs **2a** and **2c**, having both higher volume fraction of the rigid [N=P($O_2C_{12}H_8$)] block than that of **2b**, in which the aggregation is less intensive. Therefore, the presence of longer rigid [N=P($O_2C_{12}H_8$)] blocks in **2a** and **2c**, favours the chain aggregation by aromatic π-π-interactions between the [N=P($O_2C_{12}H_8$)] units. Those π-π-interactions, observed previously in cyclic 2,2'-dioxy-1,1'-biphenyl phoshazenes [23] and chiral polyphosphazenes with similar binaphtoxy phosphazene units,[24] explain the significantly different sizes of the aggregates formed by BCPs **2a-c** in THF (**2c** > **2a** > **2b**, being that proportional to the volume fraction of the rigid [N=P($O_2C_{12}H_8$)] block (see Table 1). The DLS size distribution of the 5 mg / mL solutions of BCPs **2a-c** in THF showed two peaks at very similar values of the $D_{h,App}$ than that previously obtained for the more concentrated 10 mg / mL solution. However, the intensity of the peaks were different, being the most intense those at low values of the $D_{h,App}$ (i.e. the peaks corresponding to the solvated chains of the BCPs **2a-c**, see Figure S2). When the concentration was raised to 20 mg / mL, the solution became cloudy after 12 hours evidencing the presence of very large aggregates, $D_{h,App}$ > 5000 nm, by DLS. The nature of the aggregates in solution was analysed by TEM, SEM and AFM.

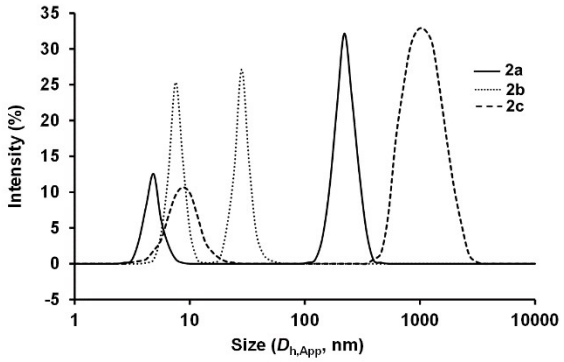

Figure 2. Dynamic light scattering traces of THF solutions (10 mg mL^{-1}) of BCPs **2a-c**.

Self-assembly of BCP 2a in thin films. The direct drop-casting of a solution of **2a** in THF (10 mg mL^{-1}) onto an appropriate solid substrate (see Experimental Part), generated a thin film with round-shaped macropores (see SEM image in Figures 3a and, TEM, AFM and additional SEM images in Figure S3) very

regular in shape and size (number average diameter of D_n = 201 nm and D_w / D_n = 1.18 (number of objects measured, N = 500. See histogram in Figure S4). These pores were generated with almost identical size and shape independently of the solid substrate used for the film formation (i.e. glass for the SEM, carbon coated copper grids for the TEM, and silicon wafer for the AFM), which evidences that the pore formation was not affected by the surface affinities of both blocks for each solid substrate.

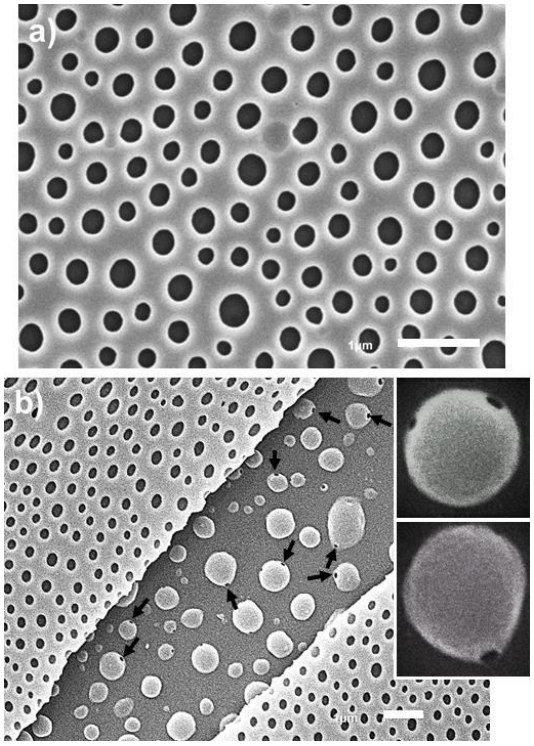

Figure 3. (a) SEM image of porous films prepared by drop-casting of a THF (10 mg mL^{-1}) solution of the BCP **2a**. Inset scale bar corresponds to 1 µm. (b) SEM image showing vesicles with holes in the wall (see black arrows) located over the glass surface in a crack of the film. The inset pictures showed these vesicles at higher magnification. The porous film is observed in the right-down and left-up corners of the picture (inset scale bar corresponds to 1 µm).

However, as a minor structure, isolated spherical aggregates were observed in regions near the edge of the films, and especially in areas where the film was missing (see SEM image in Figures 3b and, TEM and AFM in Figure 4). Those spherical aggregates had a number average diameter of D_n = 323 nm and D_w / D_n = 1.65 (N = 135, see histogram in Figure S5). Moreover, a thin dark capsule wall of *ca.* 50 nm could be detected in a high magnification bright field TEM image (Figure 4a). Remarkably, these vesicles retained their spherical shapes after the THF evaporation. All these features are consistent with a vesicle structure in which the capsule-wall is formed by the rigid [N=P($O_2C_{12}H_8$)] block, whereas the [N=PMePh] block generating is located at the inner and outer part of the corona stabilizing the vesicles in solution. Indeed, we did not observe the toroidal-shaped aggregates usually obtained when vesicles collapse during the solvent drying.[25] The location of the vesicles (outside the film), and the similarity of their sizes (*ca.* 323 nm), with that of the aggregates observed in solution by DLS ($D_{h,app}$ = 341 nm), suggested that the latter were actually vesicles (further confirmation by cryo-TEM experiments was not possible because of technical difficulties created by the THF vitrification). The proposed structure of the vesicles is depicted in the inset image of Figure 4a.

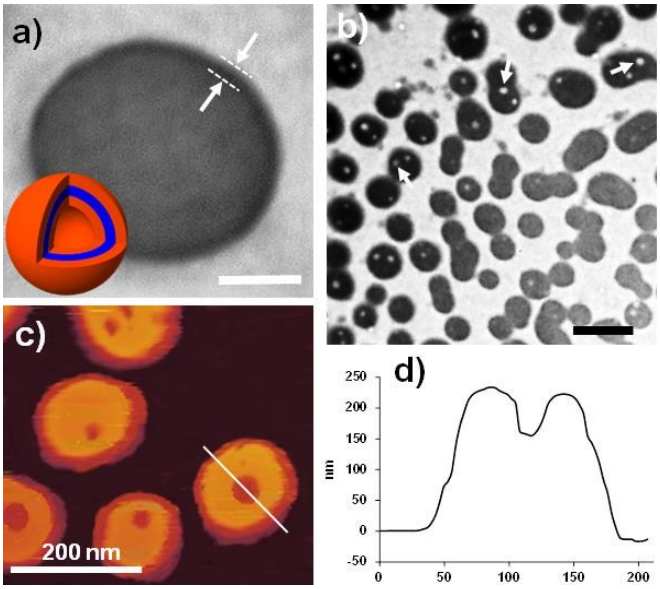

Figure 4. Vesicles of BCP **2a**. (a) Bright field TEM image at high magnification. The capsule wall can be seen as a thin dark area denoted by white arrows (inset scale bar corresponds to 100 nm). In the inset picture is showed a graphical representation of the vesicle. ([N=P($O_2C_{12}H_8$)] block in blue and [N=PMePh] block in orange). (b) Bright field TEM picture showing round holes in the membrane (see white arrows). Inset scale bar corresponds to 600 nm. (c) AFM height image. (d) Cross-sectional height profiles across one vesicle and one of the holes in the membrane.

Moreover, both SEM and TEM showed holes in the vesicle membranes (see darker round regions marked with black arrows in Figure 3b, and lighter round regions marked with white arrows in Figure 4b). The AFM cross-sectional height profiles across these holes (Figures 4c and 4d) gave a diameter of *ca.* 25 nm and a depth of *ca.* 60 nm. As this latter was slightly larger than the vesicle wall width (*ca.* 50 nm), it is clear that the holes go through the vesicle membrane and therefore, they might be produced during the evaporation of the THF retained in the inner part (we used spin-coating techniques at different rotational speeds and saturated atmosphere of THF during the film formation to study the influence of the THF evaporation rate over the formation of these holes in the capsule-wall of the vesicle. Under these experimental conditions no vesicles were observed, and the pores were the only structure present (see the explanation of the drop casting experiments later)).

When the more diluted (5 mg /mL) solution of BCP **2a** was drop-casted onto a glass substrate, the SEM showed the presence of no regular porous films (size and shape, see SEM image in Figure S6, D_n = 236, D_w / D_n = 1.85). However, the drop-casting of more concentrated solution (20 mg /mL) resulted in the formation of a very thick and homogeneous film in which no pores, nor any other nanostructures, were detected (see SEM image in Figure S7). It is clear, therefore, that, similarly to the chiral block copolyphosphazene **1**,[18] the

optimized concentration to produce regular (size and shape) pores using the BCP **2a** is 10 mg / mL.

The detailed morphology of the pores of BCP **2a** was revealed in the film cross fractures. The SEM images (see Figure 5a) showed the pores at the surface with an inverted mushroom-shape instead of the hemispherical-shape predicted by Fahmi, Nova and collaborators.[16,17]

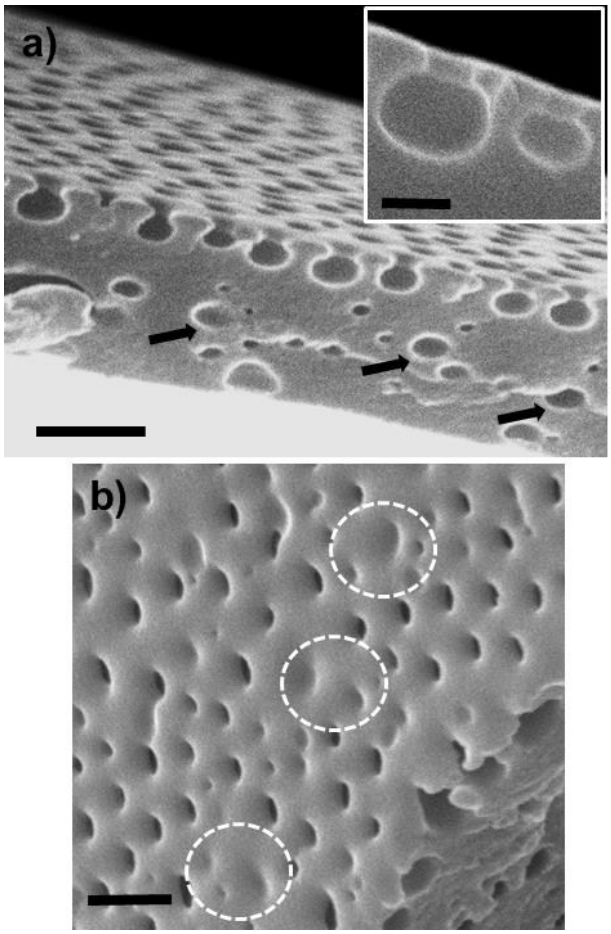

Figure 5. a) SEM image of a cross fracture of the film of BCP **2a** showing the inverted mushroom-shaped pores (detailed pore structure is showed in the inset SEM picture, inset scale bar corresponds to 200 nm). See also voids in the inner part of the film (black arrows). Inset scale bar corresponds to 1 µm. (b) SEM micrograph showing partially collapsed pores or dimples (see white dashed circle areas) at the top-surface of the film (inset scale bar corresponds to 1 µm).

The pores had an average depth of *ca.* 315 nm, being the connection between the spherical body and the top-surface of the film (stem of the mushroom) of approx. 55 nm. Their underneath diameter (*ca.* 310 nm) was larger than the open diameter in the top-surface (*ca.* 200 nm), but very similar to the average diameter of the vesicles of **2a** in solution (*ca.* 340 nm), and to those of the vesicles detected in outside the film (*ca.* 325 nm). Therefore, those pores might be originated by vesicles located just underneath the top-surface of the film. Moreover, perfect spherical voids originated by vesicles were also observed in the interior part (see black arrows in Figure 5a), evidencing that vesicles were distributed all along the thickness of the film but only those very close to the top-surface layer (*ca.* 55 nm corresponding to the stem of the mushroom) were able to originate a visible pore through the formation of connections with the surface of the film (stem of the mushroom). In fact, the free volume (void) inside the film created by the hollow spherical aggregates after the solvent evaporation should provide the driving force for the pore formation at the film top-surface. Consistently, we observed partially collapsed top-surface areas where the final pore structure was still not created (the dimples marked by dashed white circles in Figure 5b). This fact evidenced that voids originated by the vesicles produce the crash-down of the layer located just over the void leading to the observed dimple.

Interestingly, the film formed over the glass substrate used for SEM experiments can be manually separated as a brittle white powder by using a blade. The SEM analysis of this powder showed that the top-surface of the film underwent an spontaneous pilling-off from the entire film structure, generating porous flexible sheets similar to those observed by Lee and co-workers during the self-assembly of dumbbell-shaped amphiphiles (Figure 6a and Figure S8).[26]

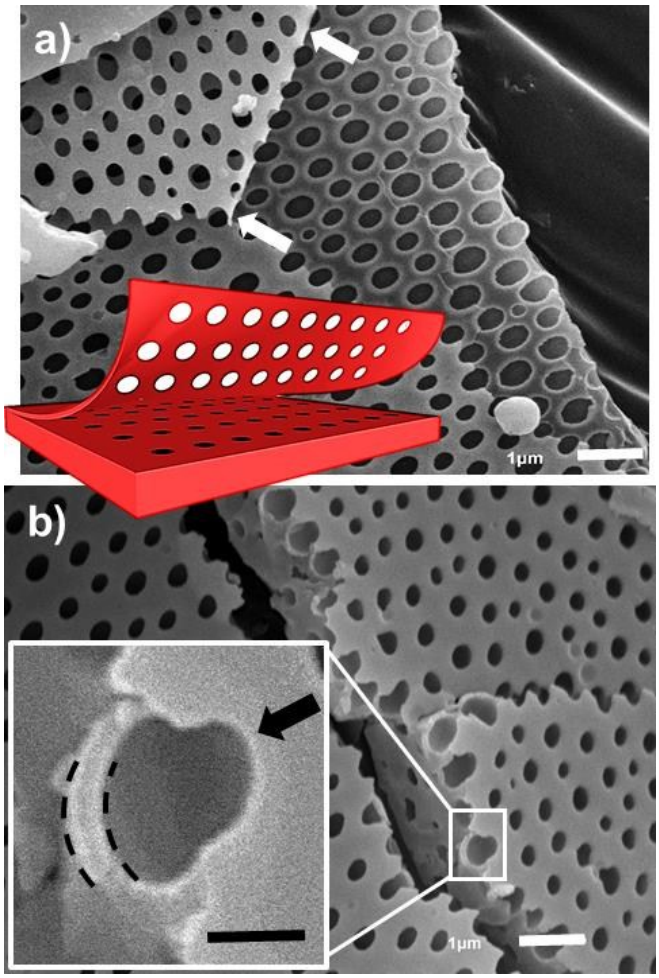

Figure 6. (a) Pilling-off the top-layer of the porous film generating a porous flexible sheet (see white arrow) and showing hemispherical pores underneath (scale bar corresponds to 1 µm). A graphical representation of the pilling-off is represented in the inset picture. (b) Detailed structure of the underneath hemispherical pores. High magnification SEM image is showed in the inset picture (see black dashed lines). The top-layer film is highlighted with a black arrow (inset scale bar corresponds to 200 nm).

Although the formation of these porous flexible sheets is still under investigation in our group, it is reasonable to think than

those were created by the separation of a layer corresponding to the connectivity between the interior spherical void and the surface of the film (i.e. having a thickness of the stem of the mushroom, *ca.* 55 nm). Accordingly, the peeling-off revealed the internal structure of the pores underneath being that close to the hemispherical-shaped (see black dashed lines in the inset picture of Figure 6b and Figure S8) proposed by Novak, Fahmi, and collaborators.[16,17] The wall thickness of these interior hemispherical pores was *ca.* 65 nm, very close to the vesicle membrane thickness determined by TEM (*ca.* 50 nm, Figure 4a), which supported that effectively the interior void was created by the vesicles originated in solution.

All these observations allowed us to propose the pathway presented in Figure 7 to explain the spontaneous formation of porous films by the self-assembly of rod-coil block copolymer **2a** through the vesicle-to-pore morphological evolution.

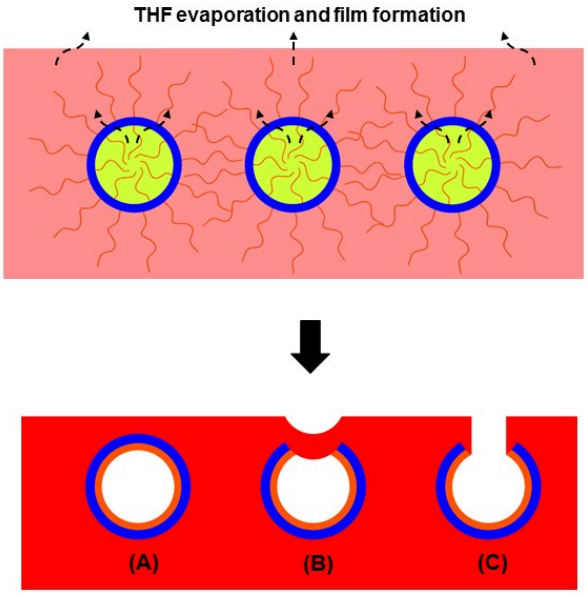

Figure 7. Proposed pathway for the spontaneous formation of porous films of block copolymer **2a** based on the presence of vesicles in solution. Rigid [N=P($O_2C_{12}H_8$)] block is depicted in blue whereas [N=PMePh] segment is in orange.

The film was created by the solvated chains of **2a** (observed in the DLS diameter distribution plot as a peak at $D_{h,App}$ = 5 nm, see Figure 2), and the close packing of vesicles during the evaporation of the THF. Thus, vesicles having THF in the inner part (solvent pools) were trapped inside of the film. The evaporation of the THF occluded in the inner part induces holes in the capsule wall and therefore voids inside the film (situation (A) in Figure 7). Those voids cause the collapsing-down of the top-layer surface just over each void originating dimples (situation (B) in Figure 7), which finally led to inverted mushroom-shaped structure of the pores (situation C in Figure 7). Experimental evidences explaining the vesicle packing to originate the film as well as how the opening of dimples occurs to create the final pore, were not found in the self-assembly of **2a**. However, those two important steps could be directly observed in the self-assembly of BCPs **2b** and **2c** having respectively shorter and longer rigid block than that of **2a** (see bellow).

Assuming the pathway described in Figure 7 for the vesicle-to-pore morphological evolution, it is clear that the process should be influenced by the solvent evaporation rate when spin-coating techniques are employed. Thus, for BCP **2a** three different rotational speeds were tested (1000, 3000 and 5000 rpm) and the results are summarized in Table 2. The SEM analysis (Figure S9) revealed the presence of round-shaped pores with a very homogeneous size distribution (D_w / D_n = 1.04) in all the samples (see histograms in Figure S10). However, the diameter of the pores decreased with higher rotational speeds (i.e., higher evaporation rates), varying from *ca.* 120 nm (film thickness of 267 nm) to *ca.* 80 nm (film thickness of 136 nm). High rotational speed (i.e., high solvent evaporation rate) hampered the vesicle-to-pore morphological evolution by freezing the pore formation and, therefore, leading to smaller pore diameters. Thus, the spin-coating technique applied to THF solutions of BCP **2a** is a convenient method for the non-template generation of macroporous films with diameters varying in the range of ~80-120 nm.

Table 1. Pore data of films of BCP 2a obtained at various rotational speeds by spin-coating.

rpm	Film thickness (nm)[a]	D_n (nm)[b]	D_w / D_n[c]
1000	267	117	1.09
3000	189	99	1.06
5000	136	82	1.12

[a] Determined by AFM analysis. [b] Diameter of the pore at the surface of the film. [c] Polydispersity calculated by measuring 213 (1000 rpm), 108 (3000 rpm) and 156 (5000 rpm) pores respectively.

Stability of pores of BCP 2a. We study the stability of the pores by heating (under vacuum) the films at 100° C, temperature that ensures the chain mobility of the flexible block (T_g *ca.* 37° C) while maintaining the rigidity of the [N=P($O_2C_{12}H_8$)] segment (T_g *ca.* 130° C). After 8 h no changes were observed in size and shape of the pores (see Figure S11 for SEM micrographs). This fact supported that the structure of the pore is built by the rigid [N=P($O_2C_{12}H_8$)] blocks, which is consistent with the proposed location of the rigid block at the membrane of the vesicles. Moreover, when the films were heated at 190° C, i.e. over the T_g of the rigid segment, the porous structure completely disappeared into an isotropic ill-defined film (see Figure S12).

We also performed a solvent annealing by keeping porous films of BCPs **2a** in a closed chamber under saturated atmosphere of THF (a good solvent for both blocks) for 10 days. The porous films evolved to nanospheres of a number average diameter of 74 nm and D_w / D_n = 1.12 (N = 135, see TEM and histogram in Figure S13 and S14 respectively). We also performed solvent annealing by keeping porous films of BCPs **2a** in a closed chamber under saturated atmosphere of THF (a good solvent for both blocks). After 10 days, the porous films evolved to nanospheres, which, at least for a period of 1month, were stable under a solvent annealing (THF) conditions. These nanospheres exhibited a number average diameter of 74 nm and D_w / D_n = 1.12 (N = 135, see TEM and histogram in Figure S13 and S14 respectively). Similar morphological evolution was previously observed with the chiral block copolymer **1**.[18] As the structure of the pore is

built by the rigid [N=P($O_2C_{12}H_8$)] block, it is reasonable that those are located at the core of the nanosphere, whilst the [N=PMePh] blocks are part of the structure of the film. Thus, under the conditions permitting the chain mobility (T = 190° C or THF atmosphere), the porosity of these materials is vanished, showing that the pores are not the thermodynamically stable nanomorphologies, and that their formation should be facilitated by the presence of the rigid [N=P($O_2C_{12}H_8$)] blocks. As it was previously mentioned, the self-assembly of BCPs **2b** and **2c** provided with important experimental evidences to explain the opening of the pores at the top-surface layer of the film (BCP **2b**), and supporting the formation of the film by close packing of vesicles during the THF evaporation (BCP **2c**).

Self-assembly of BCP 2b in thin films. The self-assembly of BCP **2b** in which the volume fraction of the rigid [N=P($O_2C_{12}H_8$)] block was significantly smaller (φ[N=P($O_2C_{12}H_8$)] = 0.28) than that of **2a** (φ[N=P($O_2C_{12}H_8$)] = 0.66), led to round porous films under the same conditions previously described for **2a** (see SEM and TEM pictures in Figure S15). The diameter of the pores of **2b** determined by SEM (D_n = 58 nm, D_w / D_n = 1.21, N = 95, see histogram in Figure S16) was closed to the size of the aggregates observed in solution by DLS ($D_{h,App}$ *ca.* 60 nm), supporting that the pores were originated by the presence of vesicles in solution in a similarly way previously described for BCP **2a**. Significantly, film regions were found in which the top-surface layer was teared over the voids generated by the vesicles underneath. In fact, lighter circular shapes corresponding to voids covered by a thin layer of film (illustration (1) in Figure 8) along with totally opened round pores at the film surface (illustration (2) in Figure 8), were clearly visible. Importantly, several cracks in the top-surface layer along the voids were also observed (see illustration (3) in Figure 8 and high magnification TEM picture at right-down side of Figure 8), indicating the tearing of the top-surface film just over the voids.

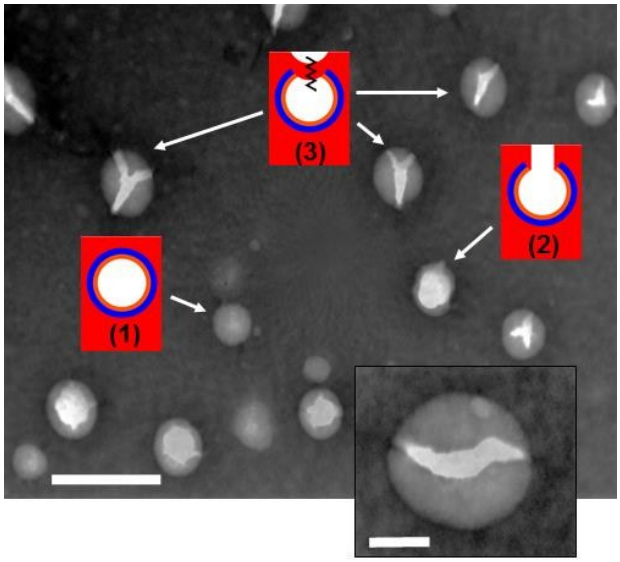

Figure 8. Different stages during the pore formation at the film surface: (1) Voids covered by a thin layer of film. (2) Opened round pores at top-layer surface. (3) Tearing of the top-surface film over the voids (see white dashed areas). Inset scale bars represent 100 nm. The right-down TEM image showed a higher magnification picture of the tearing of the top-layer film over the voids (inset scale bar corresponds to 25 nm).

This observation provided us with convincingly experimental evidences to explain the generation of the final pores at the surface of the film. Accordingly, the tearing of the film after the generation of the dimples over the voids, lead to round pores at the surface of the film that are connected with the spherical void located underneath the top layer.

Self-assembly of BCP 2c in thin films. Under the same experimental conditions used for BCP **2a** and **2b**, BCP **2c**, having a the highest volume fraction of the rigid block (φ[N=P($O_2C_{12}H_8$)] = 0.85), self-assembled into two different pore morphologies: roughly circular macropores, that were mainly concentrated in regions near the edge of the film (i.e., the areas where the film is thinner, Figure 9a); and worm-like networks with 3D interconnected pores, mostly located in the centre of the film (areas where the film is thicker, Figure 9c). Moreover, these two different pore morphologies coexisted in the intermediate film areas (Figure 9b). The size distribution of the roundish pores was significantly less uniform than that of the BCP **2a**, and so was their shape. The smallest pores (70-90 nm diameter) were almost round whereas the bigger ones had an oval pore shape, with number average pore breadth (371 nm, B_w/B_n = 1.67) and a length (514 nm, L_w/L_n = 1.83) significantly bigger than those observed in the self-assembly of BCP **2a** and **2b**.

The presence of round-shaped pores and worm-like networks with interconnected 3D pore structure in different radial regions of BCP **2c** drop-casted films, seemed to be related to the inhomogeneity in the film thickness. It is known that the self-assembled morphology depends on the film thickness [27] The reduced chain mobility during the solvent evaporation in the self-assembly of BCP **2c**, which is due to the presence of the highest volume fraction of the rigid block (φ[N=P($O_2C_{12}H_8$)] = 0.85), leads to less homogeneous film thickness than in the case of BCPs **2a** and **2b**. This fact explains the formation of different morphologies depending of the region of the film (*i.e.* the thickness of the film) in BCP **2c**. To produce films with uniform thickness, and therefore a single and pure pore morphology, we used the spin-coating technique. Thus, when the THF solution of BCP **2c** was spin-coated at 500 rpm, pure worm-like networks with continuous 3D pore structure were obtained (Figures 9d and S17, due to the lack of homogeneity of the film, the thickness could not be measured). On the other hand, pure round-shaped macropores (D_n = 83 nm, D_w/D_n = 1.25) were exclusively observed in the film (~172 nm thick) obtained at 5000 rpm (Figures 9e and S17). This fact is in aggrement with the observations previously made for the drop-casted film, confirming that BCP **2c** self-assembled preferentially into worm-like networks with continuous porous structure when the film is thicker, whereas the formation of round-shaped macropores was favored as the film became thinner.

Journal Name

ARTICLE

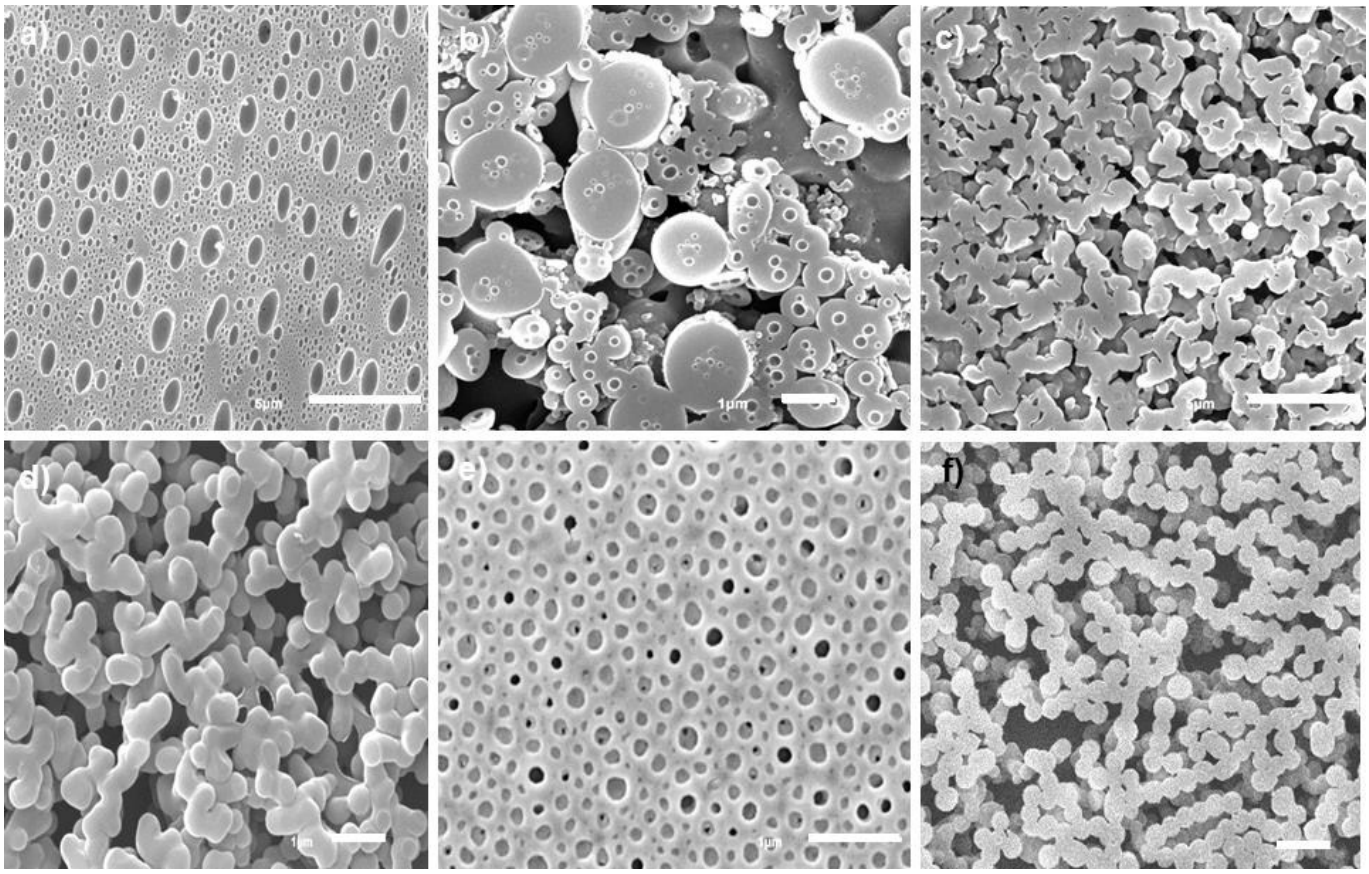

Figure 9. SEM images of porous films showing different pore morphologies in the same film prepared by drop-casting of a **2c** solution (10 mg mL^{-1} in THF). a) roundish-shaped macropores (inset scale bar represents 5 µm); b) round-shaped macropores and worm-like continuous pore structure (inset scale bar corresponds to 1 µm); c) interconnected worm-like 3D porous network (inset scale bar represents 5 µm). SEM of films prepared by spin-coating at different rotational speeds: d) at 500 rpm showing exclusively 3D pore networks and e) at 5000 rpm showing exclusively round-shaped pores (inset scale bars correspond to 1 µm); f) High magnification SEM of 3D pore network generated at 1000 rpm showing the coalescence of vesicles (inset scale bar correspond to 2 µm).

A detailed study using higher magnification SEM images of the 3D pore structure revealed than that is caused by the coalescence of spherical vesicles such as those clearly distinguished in the SEM pictures (see Figure 9f showing a higher magnification selected area). The individual vesicles have an average diameter of *ca.* 1200 nm, very similar to the $D_{h,app}$ (1151 nm) obtained by DLS for the aggregates of **2c** in THF. Therefore, the presence of a longer rigid [N=P($O_2C_{12}H_8$)] block in **2c** (245 repeated units) with respect to that of **2a** (50 repeated units) stabilized the vesicles structure during the solvent evaporation, hampering the film formation in regions where the film is thicker. This is observation is rather important since allowed us to observe the internal structure of the film before it was constructed, being that formed by the coalescence of previously created spherical vesicles.

Conclusions

A vesicle-to-pore morphological evolution has been proposed to explain the spontaneous formation of pores during the self-assembly of the BCP **2a** in thin films, [N=P($O_2C_{12}H_8$)]$_n$-*b*-[N=PMePh]$_m$ (n = 50, m = 35). The presence of the rigid [N=P($O_2C_{12}H_8$)]$_n$ segment favours the formation of stable vesicle aggregates in THF solutions that retains their spherical-shaped during the THF evaporation and formation of the film. However, the presence of pores in the capsule-wall of the vesicles evidences their tendency to generate round-shaped pores during the evaporation of THF occluded in the inner part (solvent pools). During the casting, the film is generated by closely packed vesicles, which are trapped inside, principally close to the top-layer surface, providing large amount of free volume. During the evaporation of the THF occluded in the

inner part of the vesicles, voids were created inside the film. The final structure of the pores (inverted mushroom-shape) is created when the top-surface layer of the film over each void is teared leading to round-shaped holes at the top-layer surface connected with the perfectly spherical interior voids. The self-assembly of BCP **2b**, $[N=P(O_2C_{12}H_8)]_n$-*b*-$[N=PMePh]_m$ (n = 20, m = 70), with the shortest rigid block, allowed us to observe the tearing of the top-surface layer over the voids during the THF evaporation. The self-assembly of BCPs **2c**, $[N=P(O_2C_{12}H_8)]_n$-*b*-$[N=PMePh]_m$ (n = 245, m = 60), having longer rigid block, showed the internal structure of the film which is formed by a coalescence of spherical vesicles previously produced in solution. Moreover, it was possible to create 3D interconnected pore structures or round porous films by controlling the film thickness during the casting of the THF solutions of **2c** using spin-coating techniques. Thus, whereas pure round-shaped porous films were favoured in very thin films (high rotation speed), 3D pores were obtained when thick films were prepared (low rotational speed). Under conditions that favours the chain mobility (solvent or thermal annealing over the T_g of both blocks), pores of BCP **2a** were vanished evidencing that pores were a kinetically trapped morphology probably stabilized by the presence of the rigid block. Finally, the diameter of the pores generated by the self-assembly of BCP **2a** could be adjusted from ~120 nm to ~80 nm by controlling the speed of solvent evaporation using spin-coating techniques. Future work will focus on the permeability of the films and the improving of the regularity of the pore pattern (e.g. by controlling the size of the vesicles using different solvents or solvent mixtures).

Acknowledgements

The authors are grateful to FICYT (Projects SV-PA-13-ECOEMP-83 and FC-15-GRUPIN14-106), Universidad de Oviedo (Project UNOV-13-EMERG-GIJON-08) and the MINECO (Project CTQ2014-56345-P) for the funding. We are also grateful to the COST action Smart Inorganic Polymers (SIPs-CM1302 - http://www.sips-cost.org/home/index.html). APS would like to thank the MEC for the Juan de la Cierva and Ramón y Cajal programs. SSS is grateful to the MEC for the FPU grant. We would like also to thank Alberto Álvarez Fernández for his assistance in the spin-coating experiments.

Notes and references

Materials. BCPs **2a-c** were synthesized following a previously reported methodology.[19]

Equipment. SEM studies were performed using a MEB-JEOL-6610LV microscope. Bright-field TEM micrographs were obtained on a JEOL-2000-EX-II microscope operating at 160 kV and equipped with a GATAN digital camera. Contact mode height and phase AFM images were obtained by using a Nanotec Cervantes SPM. Olympus Silicon Nitride AFM tips with less than 20 nm tip radii were employed. For the statistical size analysis, nanostructures were traced manually using ImageJ software (http://rsb.info.nih.gov/ij/) to determine the diameter length. Each micrograph was analysed completely in order to reduce subjectivity. The spin-coated films were prepared by using a SPIN 150 Spinner (SPS, Holland). Dynamic light scattering measurements were performed using a Malvern Zetasizer Nano Series running DTS (Dispersion Technology Software) software and operating a 4 mW He Ne laser at 633 nm. Analysis was performed at an angle of 173° and a constant temperature of 25 °C, using 1 cm glass cuvettes.

From this data, D_n and D_w (pore average diameter) were calculated as show bellow.

$$Dn = \frac{\sum_{i=1}^{n} NiDi}{\sum_{i=1}^{n} Ni} \qquad Dw = \frac{\sum_{i=1}^{n} NiDi^2}{\sum_{i=1}^{n} NiDi}$$

D = diameter of the object. N = number of objects

Sample preparation for self-assembly studies: The sample solutions were prepared using micro-filtered HPLC-grade THF and dissolved using an ultrasonic cleaning bath operating at 35 kHz and 160 W.

Preparation of drop-casted films: The samples were prepared by direct casting of one drop (ca. 10 µl) of BCPs **2a-c** solutions onto: a) a clean piece of glass (ca. 5x5 mm) and coated with gold for SEM analysis; b) a carbon-coated copper grid which was placed on a piece of filter paper to remove excess solvent for TEM analysis; c) a silicon wafer for AFM analysis.

The films thickness was extracted from the cross-section profile of an abruptly ended step on the film.

No staining of TEM samples was necessary, however, a RuO_4 stain was performed before the analysis in order to enhance the contrast. The water solution of RuO_4 was freshly prepared before every stain process by treatment of 20 mg of $RuCl_3$ with 1 mL of sodium hypochlorite (10 % solution in water). The samples were stained for 2 hours.

1 W. G. Bae, H. N. Kim, D. Kim, S. H. Park, H. E. Jeong and K. Y. Suh, *Adv. Mater*, 2014, **26**, 675.

2 (a) M. Trau, N. Yao, E. Kim, Y. Xia, G. M. Whitesides and I. A. Aksay, *Nature,* 1997, **390**, 674; (b) C. Zhao, E. Danish, N. R. Cameron and R. Kataky, *J. Mater. Chem.,* 2007, **17**, 2446; (c) M. S. Silverstein, H. Tai, A. Sergienko, Y. Lumelsky and S. Pavlovsky, *Polymer,* 2005, **46**, 6682.

3 (a) J. Huang, C. Tao, Q. An, W. Zhang, Y. Wu, X. Li, D. Shen and G. Li, *Chem. Commun*., 2010, **46**, 967; (b) X. Hu, G. Li, M. Li, J. Huang, Y. Li, Y. Gao and Y. Zhang, *Adv. Funct. Mater.,* 2008, **18**, 575.

4 (a) F. Schacher, M. Ulbricht and A. H. E. Müller, *Adv. Funct. Mater.,* 2009, **19**, 1040; (b) E. A. Jackson and M. A. Hillmyer, *ACS Nano,* 2010, **4**, 3548; (c) X. Wang, S. M. Husson, X. Qian and S. R. Wickramasinghe, *J. Membr. Sci.,* 2010, **365**, 302; (d) W. Phillip, J. Rzayev, M. Hillmyer and E. Cussler, *J. Membr. Sci.,* 2006, **286**, 144; (e) W. A. Phillip, B. O´Neill, M. Rodwogin, M. A. Hillmyer and E. L. Cussler, *ACS Appl. Mater. Interfaces,* 2010, **2**, 847; (f) H. Uehara, M. Kakiage, M. Sekiya, D. Sakuma, T. Yamonobe, N. Takano, A. Barraud, E. Meurville and P. Ryser, *ACS Nano,* 2009, **3**, 924; (g) S. Y. Yang, I. Ryu, H. Y. Kim, J. K. Kim, S. K. Jang and T. P. Russell, *Adv. Mater.,* 2006, **18**, 709; (h) S. Y. Yang, J. A. Yang, E. S. Kim, G. Jeon, E. J. Oh, K. Y. Choi, S. K. Hahn and J. K. Kim, *ACS Nano,* 2010, **4**, 3817; (i) S. Y. Yang, J. Park, J. Yoon, M. Ree, S. K. Jang and J. K. Kim, *Adv. Funct. Mater.,* 2008, **18**, 1371; (j) Y. Lv, T. C.

Hughes, X. Hao, N. K. Hart, S. W. Littler, X. Zhang and T. Tan, *Macromol. Rapid Commun.,* 2010, **31**, 1785.
5 I. Pulko, J. Wall, P. Krajnc and N. R. Cameron, *Chem. - Eur. J.,* 2010, **16**, 2350.
6 (a) C. D Wood, B. Tan, A. Trewin, F. Su, M. J. Rosseinsky, D. Bradshaw, Y. Sun, L. Zhou and A. I. Cooper, *Adv. Mater*., 2008, **20**, 1916; (b) N. Du, G. P. Robertson, J. Song, I. Pinnau, S. Thomas and M. D. Guiver, *Macromolecules,* 2008, **41**, 9656; (c) S. S. Han, H. Furukawa, O. M. Yaghi and W. A. Goddard, *J. Am. Chem. Soc.,* 2008, **130**, 11580; (d) H. Furukawa and O. M. Yaghi, *J. Am. Chem. Soc.,* 2009, **131**, 8875; (e) C. J. Doonan, D. J. Tranchemontagne, T. G. Glover, J. R. Hunt and O. M. Yaghi, *Nat. Chem.,* 2010, **2**, 235; (f) S. Yuan, S. Kirklin, B. Dorney, D. J. Liu and L. Yu, *Macromolecules,* 2009, **42**, 1554.
7 (a) Z. Shi, Y. Zhou and D. Yan, *Macromol. Rapid Commun.,* 2006, **27**, 1265; (b) G. Li, X. Yang, B. Wang, J. Wang and X. Yang, *Polymer,* 2008, **49**, 3436; (c) X. Yang, L. Chen, B. Huang, F. Bai and X. Yang, *Polymer,* 2009, **50**, 3556; (d) M. R. Abidian, D. H. Kim and D. C. Martin, *Adv. Mater.,* 2006, **18**, 405; (e) H. Duan, M. Kuang, G. Zhang, D. Wang, D. G. Kurth and H. Möhwald, *Langmuir,* 2005, **21**, 11495.
8 (a) J. X. Jiang, A. Trewin, F. Su, C. D. Wood, H. Niu, J. T. A. Jones, Y. Z. Khimyak and A. I. Cooper, *Macromolecules,* 2009, **42**, 2658; (b) X. Hu, Q. An, G. Li, S. Tao and J. Liu, *Angew. Chem., Int. Ed.,* 2006, **45**, 8145; (c) J. Rzayev and M. A. Hillmyer, *Macromolecules,* 2005, **38**, 3.
9 (a) M. Lazzari, G. Liu and S. Lecommandoux, *Block Copolymers in Nanoscience*; Wiley-VCH: Weinheim, 2006; (b) F. H. Schacer, P. A. Rupar and I. Manners, *Angew. Chem. Int. Ed.,* 2012, **51**, 7898; (c) Y. Mai and A. Eisenberg, *Chem. Soc. Rev.,* 2012, **41**, 5969.
10 (a) D. Wu, F. Xu, B. Sun, R. Fu, H. He and K. Matyjaszewski, *Chem. Rev.,* 2012, **112**, 3959; (b) M. A. Hillmyer, *Adv. Polym. Sci.,* 2005, **190**, 137.
11 (a) Y. Meng, D. Gu, F. Zhang, Y. Shi, H. Yang, Z. Li, C. Yu, B. Tu and D. Zhao, *Angew. Chem. Int. Ed.,* 2005, **44**, 7053; (b) Y. Deng, T. Yu, Y. Wan, Y. Shi, Y. Meng, D. Gu, L. Zhang, Y. Huang, C. Liu, X. Wu and D. Zhao, *J. Am. Chem. Soc.,* 2007, **129**, 1690.
12 K. Kailasam, Y.-S. Jun, P. Katekomol, J. D. Epping, W. H. Hong and A. Thomas, *Chem. Mater.,* 2010, **22**, 428.
13 Porous framework from BCP self-assembly with sacrificial component: (a) D. A. Olson, L. Chen and M. A. Hillmyer, *Chem. Mater.,* 2008, **20**, 869; (b) M. Seo and M. A. Hillmyer, *Science,* 2012, **336**, 1422. Porous framework from BCP self-assembly with morphology reconstruction (without sacrificial component): (a) Y. Wang and F. Li, *Adv. Mater.,* 2011, **23**, 2134; (b) T. Xu, J. Stevens, J. Villa, J. T. Goldbach, K. W. Guarini, C. T. Black, C. J. Hawker and T. P. Russel, *Adv. Funct. Mater.,* 2003, **13**, 698.
14 (a) J. Ding and G. Liu, *Macromolecules,* 1997, **30**, 655; (b) W. Bu, H. Li, H. Sun, S. Yin and L. Wu, *J. Am. Chem. Soc.,* 2005, **127**, 8016; (c) B. S. Li, J. Chen, C. F. Zhu, K. K. L. Leung, L. Wan, C. Bai and B. Z. Tang, *Langmuir,* 2004, **20**, 2515; (d) P.-H. Tung, S.-W. Kuo, K.-U. Jeong, S. Z. D. Cheng, C.-F. Huang and F.-C. Chang, *Macromol. Rapid Commun.,* 2007, **28**, 271; (e) P.-H. Tung, S.-W. Kuo, S.-C. Chan, C.-H. Hsu, C.-F. Wang and F.-C. Chang, *Macromol. Chem. Phys.,* 2007, **208**, 1823.
15 S. A. Jenekhe and X. L. Chen, *Science,* 1999, **283**, 372.
16 T. Pietsch, N. Gindi and A. Fahmi, *Soft Matter.,* 2009, **5**, 2188.
17 J. F. Reuther, D. A. Siriwardane, O. V. Kulikov, B. L. Batchelor, R. Campos and B. M. Novak, *Macromolecules,* 2015, **48**, 3207.
18 (a) S. Suarez-Suarez, G. A. Carriedo, M. P. Tarazona and A. Presa Soto, *Chem. - Eur. J.,* 2013, **19**, 5644; (b) S. Suarez-Suarez, G. A. Carriedo and A. Presa Soto, *Chem. - Eur. J,.* 2013, **19**, 15933.
19 S. Suarez-Suarez, D. Presa Soto, G. A. Carriedo, A. Presa Soto and A. Staubitz, *Organometallics,* 2012, **31**, 2571.
20 (a) C. H. Honeyman, I. Manners, C. T. Morrissey and H. R. Allcock, *J. Am. Chem. Soc.,* 1995, **117**, 7035; (b) H. R. Allcock, J. M. Nelson, S. D. Reeves, C. H. Honeyman and I. Manners, *Macromolecules,* 1997, **30**, 50; (c) H. R. Allcock, S. D. Reeves, J. M. Nelson, C. A. Crane and I. Manners, *Macromolecules,* 1997, **30**, 2213.
21 G. A. Carriedo, P. Gómez-Elipe, F. J. García-Alonso, E. Lizaso, M. E. Muño and, A. Santamaría, *Macromol. Chem. Phys.,* 2001, **202**, 3437.
22 The homopolymers $[N=P(O_2C_{12}H_8)]_n$ and $[N=PMePh]_n$ presented in the block copolymers **2a-c** are soluble in THF. $[N=P(O_2C_{12}H_8)]_n$: (a) G. A. Carriedo, L. Fernández-Catuxo, F. J. García-Alonso, P. Gómez-Elipe, and P. A. González, Macromolecules, 1996, **29**, 5320. (b) G. A. Carriedo, F. J. García-Alonso, P. A. González, J. L. García Álvarez, and P. Gómez-Elipe, Phosphorus, Sulfur and Silicon, 1999, **73**, 144. $[N=PMePh]_n$: (a) R. H. Neilson and P. Wisian-Neilson, Chem. Rev. 1988, **88**, 541. (b) P. Wisian-Neilson and G.-F. Xu, Macromolecules 1996, **29**, 3457. Moreover, DLS experiments, performed by using both homopolymers at 10 mg / mL in THF (i.e., the same concentration and solvent previously used for BCPs **2a-c**), showed only one peak at low $D_{h,App}$ values (7 nm the rigid $[N=P(O_2C_{12}H_8)]_n$, and 4 nm the $[N=PMePh]_n$ block), evidencing the absence of aggregates in those THF solutions.
23 J. L. García Álvarez, M. E. Amato, G. M. Lombardo, G. A. Carriedo and F. Punzo, *Eur. J. Inorg. Chem.,* 2010, 4483.
24 S. Suarez-Suarez, G. A. Carriedo and A. Presa Soto, *Chem. - Eur. J.,* 2015, **21**, 14129.
25 (a) J. Du, Y. Chen, Y. Zhang, C. C. Han, K. Fischer and M. Schmidt, *J. Am. Chem. Soc.,* 2003, **125**, 14710; (b) W. Tao, Y. Liu, B. Jiang, S. Yu, W. Huang, Y. Zhou and D. Yan, *J. Am. Chem. Soc.,* 2012, **134**, 762; (c) J. Zou, B. Guan, X. J. Liao, M. Jiang and F. G. Tao., *Macromolecules,* 2009, **42**, 7465.
26 E. Lee, J.-K. Kim and M. Lee, *Macromol. Rapid Commun.,* 2010, **31**, 975.
27 A. Knoll, A. Horvat, K. S. Lyakhova, G. Krausch, G. J. A. Sevink, A. V. Zvelindovsky, and R. Magerle, *Phys. Rev. Lett.*, 2002, **89**, 35501.

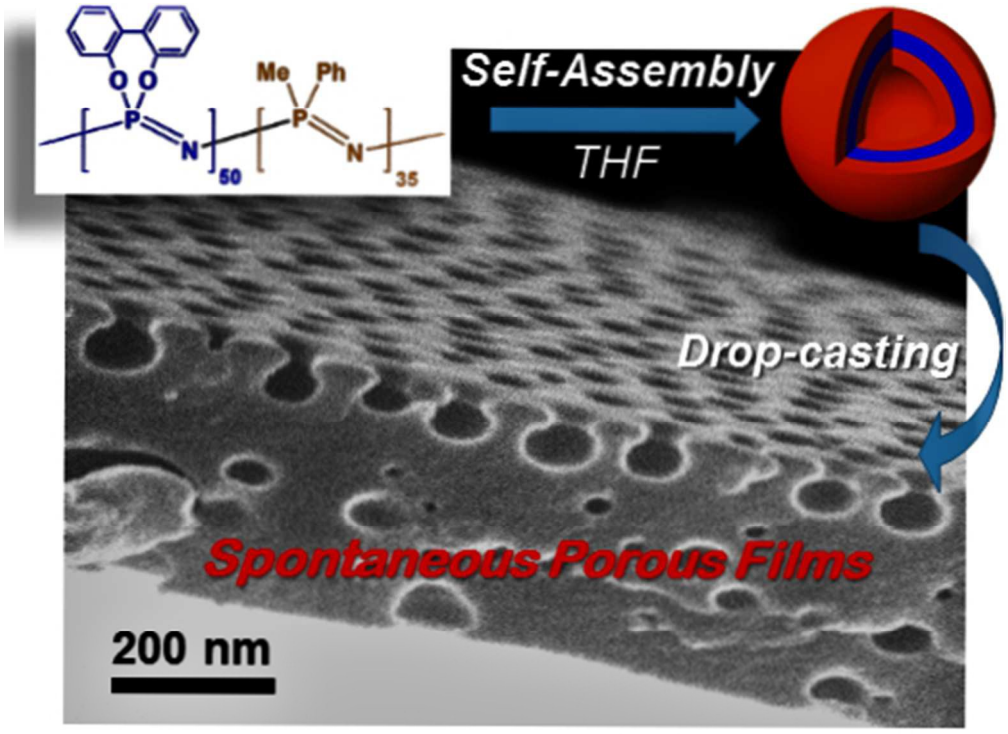

137x100mm (96 x 96 DPI)